



14 **Abstract**

15 Learning effectively from errors requires using them in a context-dependent manner, for example  
16 adjusting to errors that result from unpredicted environmental changes but ignoring errors that  
17 result from environmental stochasticity. Where and how the brain represents errors in a context-  
18 dependent manner and uses them to guide behavior are not well understood. We imaged the  
19 brains of human participants performing a predictive-inference task with two conditions that had  
20 different sources of errors. Their performance was sensitive to this difference, including more  
21 choice switches after fundamental changes versus stochastic fluctuations in reward contingencies.  
22 Using multi-voxel pattern classification, we identified context-dependent representations of error  
23 magnitude and past errors in posterior parietal cortex. These representations were distinct from  
24 representations of the resulting context-dependent behavioral adjustments in dorsomedial frontal,  
25 anterior cingulate, and orbitofrontal cortex. The results provide new insights into human brain  
26 that represent and use errors in a context-dependent manner to support adaptive behavior.

27

## 28 **Introduction**

29           Errors often drive adaptive adjustments in beliefs that inform behaviors that maximize  
30 positive outcomes and minimize negative ones (Sutton & Barto, 1998). A major challenge to  
31 error-driven learning in uncertain and dynamic environments is that errors can arise from  
32 different sources that have different implications for learning. For example, a bad experience at a  
33 restaurant that recently hired a new chef might lead you to update your belief about the quality of  
34 the restaurant, whereas a similar experience at a well-known restaurant with a chef that has long  
35 been your favorite might be written off as a one-time bad night. That is, the same errors should  
36 be interpreted differently in different contexts. In general, errors that represent fundamental  
37 changes in the environment or that occur during periods of uncertainty should probably lead you  
38 to update your beliefs and change your behavior, whereas those that result from environmental  
39 stochasticity are likely better ignored (d'Acremont & Bossaerts, 2016; Li, Nassar, Kable, & Gold,  
40 2019; Nassar, Bruckner, & Frank, 2019; O'Reilly et al., 2013).

41           Neural representations of key features of these kinds of dynamic, error-driven learning  
42 processes have been identified in several brain regions. For example, several studies focused on  
43 variables derived from normative models that describe the degree to which individuals should  
44 dynamically adjust their beliefs in response to error feedback under different task conditions,  
45 including the probability that a fundamental change in the environment just occurred (change-  
46 point probability, or CPP, which is a form of surprise) and the reducible uncertainty associated  
47 with estimates of environmental features (relative uncertainty, or RU). Correlates of these  
48 variables have been identified in dorsomedial frontal (DMFC) and dorsolateral prefrontal  
49 (DLPFC) cortex and medial and lateral posterior parietal cortex (PPC) (Behrens, Woolrich,  
50 Walton, & Rushworth, 2007; McGuire, Nassar, Gold, & Kable, 2014; Nassar, McGuire, Ritz, &  
51 Kable, 2019). These and other studies also suggest specific roles for these different brain regions  
52 in error-driving learning, including representations of surprise induced by either state changes or  
53 outliers (irrelevant to state changes) in the PPC that suggest a role in error monitoring (Nassar,  
54 Bruckner, et al., 2019; O'Reilly et al., 2013), and representations of variables more closely  
55 related to belief and behavior updating in the prefrontal cortex (PFC) (McGuire et al., 2014;  
56 O'Reilly et al., 2013). However, these previous studies, which typically used continuous rather  
57 than discrete feedback, were not designed to identify neural signals related to a key aspect of

58 flexible learning in uncertain and dynamic environments: responding to the same exact errors  
59 differently in different contexts.

60 To identify such context-dependent neural responses to errors, we adapted a paradigm  
61 from our previous single-unit recording study (Li et al., 2019). In this paradigm, we generated  
62 two different dynamic environments by varying the amount of noise and the frequency that  
63 change-points occur (i.e., hazard rate; Behrens et al., 2007; Glaze, Kable, & Gold, 2015; Nassar  
64 et al., 2012; Nassar, Wilson, Heasley, & Gold, 2010). In the unstable environment, noise was  
65 absent and the hazard rate was high, and thus errors unambiguously signaled a change in state. In  
66 the high-noise environment, noise was high and the hazard rate was low, and thus small errors  
67 were ambiguous and could indicate either a change in state or noise. Thus, effective learning  
68 requires treating errors in the two conditions differently, including adjusting immediately to  
69 errors in the unstable environment but using the size of errors and recent error history as cues to  
70 aid interpretation of ambiguous errors in the high-noise condition.

71 In our previous study, we found many single neurons in the anterior cingulate cortex  
72 (ACC) or posterior cingulate cortex (PCC) that responded to errors or the current context, but we  
73 found little evidence that single neurons in these regions combined this information in a context-  
74 dependent manner to discriminate the source of errors or drive behavior. In the current study, we  
75 used whole-brain fMRI and multi-voxel pattern classification to identify context-dependent  
76 neural responses to errors and activity predictive of context-dependent behavioral updating in the  
77 human brain. The results show context-dependent encoding of error magnitude and past errors in  
78 PPC and encoding of behavioral shifts in a large array of frontal regions including ACC, DMFC,  
79 DLPFC and orbitofrontal cortex (OFC), which provide new insights into the distinct roles these  
80 brain regions play in representing and using, respectively, errors in a context-dependent manner  
81 to guide adaptive behavior.

82

## 83 **Results**

84 Sixteen human participants performed a predictive-inference task (Figure 1A) while  
85 fMRI was used to measure their blood-oxygenation-level-dependent (BOLD) brain activity. The  
86 task required them to predict the location of a single rewarded target from a circular array of ten  
87 targets. The location of the rewarded target was sampled from a distribution based on the  
88 location of the current best target and the noise level in the current condition. In addition, the

89 location of the best target could change according to a particular, fixed hazard rate ( $H$ ). Two  
90 conditions with different noise levels and hazard rates were conducted in separate runs. In the  
91 high-noise condition (Figure 1B–C), the rewarded target would appear in one of the five  
92 locations relative to the location of the current best target, and the hazard rate was low ( $H = 0.02$ ).  
93 In the unstable condition (Figure 1D–E), the rewarded target always appeared at the location of  
94 the best target, and the hazard rate was high ( $H = 0.35$ ). On each trial, participants made a  
95 prediction by looking at a particular target, and then were given explicit, visual feedback about  
96 their chosen target and the rewarded target. Effective performance required them to use this  
97 feedback in a flexible and context-dependent manner, including typically ignoring small errors in  
98 the high-noise condition but responding to small errors in the unstable condition by updating  
99 their beliefs about the best-target location.

100

### 101 *Behavior*

102 Nearly all of the participants' choice patterns were consistent with a flexible, context-  
103 dependent learning process (closed symbols in Figure 2). On average, they learned the location  
104 of the best target after a change in its location more quickly and reliably in the unstable versus  
105 high-noise condition (Figure 2A). This flexible learning process had two key signatures. First,  
106 target switches (i.e., predicting a different target than on the previous trial) tended to follow  
107 errors of any magnitude in the unstable condition but only errors of high magnitude (i.e., when  
108 the chosen target was 3, 4, or 5 targets away from the rewarded target) in the high-noise  
109 condition (sign test for  $H_0$ : equal probability of switching for the two conditions; error magnitude  
110 of 1: median = -0.35, interquartile range (IQR) = [-0.62, -0.25],  $p < 0.001$ ; error magnitude of 2:  
111 median = -0.30, IQR = [-0.70, -0.11],  $p < 0.001$ ; Figure 2B–C). Second, target switches depended  
112 on error history only for low-magnitude errors (i.e., when the chosen target was 1 or 2 targets  
113 away from the rewarded target) in the high-noise condition but not otherwise (sign test for  $H_0$ :  
114 switching was unaffected when recent history contained fewer errors; error magnitude of 1:  
115 median = -0.29, IQR = [-0.42, -0.10],  $p = 0.004$ ; error magnitude of 2: median = -0.25, IQR = [-  
116 0.38, -0.14],  $p < 0.001$ ; Figure 2D–F).

117 We accounted for these behavioral patterns with a reduced Bayesian model that is similar  
118 to ones we have used previously to model belief updating in a dynamic environment (open  
119 symbols in Figure 2; Tables 1 and 2). According to this model, the decision-maker's trial-by-trial

120 choices are governed by ongoing estimates of the probability that the best target changed  
121 (change-point probability, or CPP) and reducible uncertainty about the best target's location  
122 (relative uncertainty, or RU). Both quantities are influenced by the two free parameters in the  
123 model, subjective hazard rate and noise level, which were fitted separately in each condition for  
124 each participant. As expected, the fitted hazard rates were higher in the unstable condition than  
125 in the high-noise condition, although both tended to be higher than the objective values, as we  
126 have observed previously (Nassar et al., 2010). The fitted noise estimates were not reliably  
127 different between the high-noise versus unstable condition (Table 2).

128         In the reduced Bayesian model, both CPP and RU contribute to processing errors in a  
129 context-dependent manner. CPP increases as the current error magnitude increases and achieves  
130 high values more quickly in the unstable condition because of the higher hazard rate (Figure 3A).  
131 These dynamics lead to a greater probability of switching targets after smaller errors in the  
132 unstable condition. RU increases on the next trial after the participant makes an error and does so  
133 more in the high-noise condition because of the lower hazard rate (Figure 3B). These dynamics  
134 lead to a greater probability of target switches when the last trial was an error, which is most  
135 prominent for small errors in the high noise condition. Thus, CPP and RU each account for one  
136 of the two key signatures of context-dependent learning that we identified in participants'  
137 behavior, with CPP driving a context-dependent influence of error magnitude and RU driving a  
138 context-dependent influence of error history on target switches (Figure 3C).

139         We also tested several alternative models but they did not provide as parsimonious  
140 descriptions of the data (Figure 2 – figure supplement 1, and Tables 1 and 2). Notably, an  
141 alternative model that assumed a condition-specific fixed learning rate also assumed errors were  
142 treated differently for the two conditions but did not include trial-by-trial adjustments of learning  
143 rates used by the reduced Bayesian model. Thus, although this model performed better than the  
144 reduced Bayesian model in the unstable condition, it cannot capture participants' behaviors in the  
145 high-noise condition, where dynamically integrating both current and past errors is required for  
146 adapting trial-by-trial behavior. Other hybrid models performed worse than the reduced Bayesian  
147 model under both conditions.

148

149 *Neural representation of CPP and RU*

150 To compare our current data directly to our previously identified neural representations of  
151 CPP and RU (McGuire et al., 2014), the two key quantities in the reduced Bayesian model, we  
152 conducted univariate analyses of our imaging data using those behaviorally derived variables as  
153 regressors. This comparison also allowed us to better isolate representations of these variables  
154 from those related to visual and motor processing demands that differed considerably for the two  
155 tasks (the other task included a more complex visual scene and used hand, not eye, movements).  
156 Similar to our previous findings, we found activity that was positively correlated with the levels  
157 of CPP and RU across DLPFC and PPC (Figure 3D). We identified these joint neural  
158 representations of CPP and RU in the high-noise condition, because both CPP and RU varied  
159 across trials in this condition, in contrast to the unstable condition in which RU did not vary. The  
160 regions of DLPFC and PPC that were responsive to both CPP and RU were a subset of those  
161 identified as showing this conjunction in our previous study (Figure 3E, Figure 3 – figure  
162 supplement 1).

163 Because CPP and RU both contribute to responding to errors in a context-dependent  
164 manner, we considered the brain regions that responded to both variables as good candidates for  
165 encoding errors in a context-dependent manner that is linked to subsequent behavioral shifts. In  
166 the following analyses, we aimed to directly identify context-dependent neural representations of  
167 error magnitude and error history, as well as activity that predicts subsequent shifts in behavior,  
168 in these and other brain regions.

169

### 170 *Context-dependent neural representation of errors*

171 We used multi-voxel pattern analysis (MVPA) to identify error-related neural signals that  
172 were similar and different for the two task conditions. Given the two key signatures of flexible  
173 learning that we identified in behavior, we were especially interested in identifying neural  
174 representations of error magnitude and past errors that were stronger in the high-noise than the  
175 unstable condition.

176 We found robust, context-dependent representations of the magnitude of the error on the  
177 current trial in PPC. Consistent with the context-dependent behavioral effects, this representation  
178 of error magnitude was stronger in the high-noise than the unstable condition (Figure 4 and  
179 Table 3). Specifically, we could classify correct versus error feedback on the current trial across  
180 almost the entire cortex, in both the unstable and noisy conditions. However, for error trials, we

181 could classify error magnitude (in three bins: 1, 2, 3+ targets away from the rewarded target)  
182 only for the high-noise condition and most strongly in the lateral and medial parietal cortex and  
183 in the occipital pole. In a parallel set of analyses, we found that univariate activity in PPC also  
184 varied in a context-dependent way, responding more strongly to error magnitude in the high-  
185 noise than the unstable condition (Figure 4 – figure supplement 1).

186 We also found robust, context-dependent representations of past errors in PPC. These  
187 representations also were stronger in the high-noise than the unstable condition, particularly on  
188 trials for which past errors had the strongest influence on behavior. Specifically, we could  
189 classify correct versus error on the previous trial in PPC for both task conditions (Figure 5). This  
190 classification of past errors depended on the outcome of the current trial. We separated trials  
191 according to whether the current feedback was correct or an error, or whether the error  
192 magnitude provided ambiguous (error magnitudes of 1 or 2) or unambiguous (error magnitudes  
193 of 0 or 3+) feedback in the high-noise condition (Figure 5). We found reliable classifications of  
194 past errors in the lateral and medial parietal cortex in both conditions for correct trials and  
195 unambiguous feedback. Moreover, these representations depended on the current context, and,  
196 consistent with behavioral effects of error history, were stronger for error trials and ambiguous  
197 feedback in the high-noise than in the unstable condition (Table 3). These context-dependent  
198 signals for past errors were not clearly present in univariate activity (Figure 5 – figure  
199 supplement 1). An additional conjunction analysis across MVPA results showed that PPC  
200 uniquely encoded context-dependent error signals for both error magnitude of the current trials  
201 and past errors when the current trial provided ambiguous feedback (Table 3).

202

### 203 *Neural prediction of subsequent changes in behavior*

204 Although PPC responds to errors in a context-dependent manner that could be used for  
205 determining behavioral updates, we did not find that activity in this region was predictive of the  
206 participants' future behavior. Instead, we found such predictive activity more anteriorly  
207 throughout the frontal lobe. Specifically, we investigated whether multi-voxel neural patterns  
208 could predict participants' target switches on the subsequent trial. We focused on the trials with  
209 small error magnitudes (1 or 2) in the high-noise condition, because these were the only trial  
210 types that participants consistently exhibited an intermediate probability of switching (20–80%,  
211 Figure 2). We found that activity patterns in widespread regions in OFC, ACC, DMFC, and



212 DLPFC could predict subsequent stay/switch decisions (Figure 6, Table 4). We did not find any  
213 regions where univariate activity reliably predicted participants' subsequent behavior (Figure 6 –  
214 figure supplement 1).

215

## 216 **Discussion**

217 We identified context-dependent neural representations of errors in humans performing a  
218 dynamic learning task. The task required participants to learn in two different dynamic  
219 environments. In the unstable condition (high hazard rate and low noise), errors unambiguously  
220 indicated a change in the state of the environment, and participants reliably updated their  
221 behavior in response to errors. In contrast, in the high-noise condition (low hazard rate and high  
222 noise), small errors were ambiguous, and participants used both the current error magnitude and  
223 recent error history to distinguish between those errors that likely signal change-points and those  
224 likely arising from environmental noise. Using MVPA, we showed complementary roles of PPC  
225 and prefrontal regions (including OFC, ACC, DMFC and DLPFC) in the outcome-monitoring  
226 and action-selection processes underlying these flexible, context-dependent behavioral responses  
227 to errors. Neural patterns in PPC encoded the magnitude of errors and past errors, more strongly  
228 in the high-noise than the unstable condition. These context-dependent neural responses to errors  
229 in PPC were not reliably linked to subsequent changes in behavior. In contrast, neural patterns in  
230 prefrontal regions could predict subsequent changes in behavior (whether participants switch  
231 their choice on the next trial or not) in response to ambiguous errors in the high-noise condition.

232

### 233 *Context-dependent behavior adaptation*

234 Consistent with previous studies of ours and others (d'Acromont & Bossaerts, 2016;  
235 McGuire et al., 2014; Nassar, Bruckner, et al., 2019; Nassar et al., 2012; Nassar et al., 2010;  
236 O'Reilly et al., 2013; Purcell & Kiani, 2016), human participants adapted their response to errors  
237 differently in different contexts. In the unstable condition, participants almost always switched  
238 their choice after errors and quickly learned the new state after change-points. In contrast, in the  
239 high-noise condition, participants ignored many errors and only slowly learned the new state  
240 after change-points. In this condition, participants had to distinguish true change-points from  
241 environmental noise, and they used error magnitude and recent error history as a cue for whether  
242 the state had recently changed or not. These flexible and context-dependent responses to errors

243 could be accounted for by a reduced Bayesian model (McGuire et al., 2014; Nassar et al., 2012;  
244 Nassar et al., 2010). In this model, beliefs and behavior are dynamically updated according to  
245 two key quantities, CPP and RU.

246

#### 247 *Neural representation of change-point probability and relative uncertainty*

248 Replicating our previous work (McGuire et al., 2014), we identified neural activity  
249 correlated with both CPP and RU in PPC and DLPFC. This replication shows the robustness of  
250 these neural representations of CPP and RU across experimental designs that differ dramatically  
251 in their visual stimuli and motor demands, yet share the need to learn in dynamic environments  
252 with similar statistics. In addition, given that CPP and RU account for the context-dependent  
253 behavioral responses to error magnitude and recent error history, respectively, the regions  
254 responding to both CPP and RU are strong candidates for neural representations of errors and  
255 subsequent behavioral updates that are context dependent.

256

#### 257 *Context-dependent neural representation of errors*

258 Advancing beyond previous work, we identified context-dependent encoding of errors in  
259 neural activity in the PPC. Mirroring the context dependence of behavior, the multivariate neural  
260 pattern in PPC encoded current error magnitude more strongly in the high-noise condition than in  
261 the unstable condition and encoded past errors more strongly on trials that provided ambiguous  
262 feedback in the high-noise condition. That is, the multivariate pattern in PPC could distinguish  
263 between the same exact error stimuli depending on the context. These same regions of PPC have  
264 been shown previously to represent errors, error magnitudes, surprise and salience (Fischer &  
265 Ullsperger, 2013; Gläscher, Daw, Dayan, & O'Doherty, 2010; McGuire et al., 2014; Nassar,  
266 Bruckner, et al., 2019; Nassar, McGuire, et al., 2019; O'Reilly et al., 2013; Payzan-LeNestour,  
267 Dunne, Bossaerts, & O'Doherty, 2013). In addition, these regions have been shown to integrate  
268 recent outcome or stimulus history in human fMRI studies (FitzGerald, Moran, Friston, & Dolan,  
269 2015; Furl & Averbeck, 2011) and in animal single neuron recording studies (Akrami, Kopec,  
270 Diamond, & Brody, 2018; Brody & Hanks, 2016; Hanks et al., 2015; Hayden, Nair, McCoy, &  
271 Platt, 2008; Hwang, Dahlen, Mukundan, & Komiyama, 2017). Our results extend on these past  
272 findings by demonstrating that the neural encoding of errors in PPC is modulated across different  
273 contexts in precisely the manner that could drive adaptive behavior.

274           These whole-brain fMRI results complement our previous results recording from single  
275 neurons in ACC and PCC in the same task (Li et al., 2019). In that study, we identified single  
276 neurons in both ACC and PCC that encoded information relevant to interpreting errors, such as  
277 the magnitude of the error or the current context. However, we did not find any neurons that  
278 combined this information in a manner that could drive adaptive behavioral adjustments. Our  
279 whole-brain fMRI results suggest that PPC would be a good place to look for context-dependent  
280 error representations in single neurons, including a region of medial parietal cortex slightly  
281 dorsal to the PCC area we recorded from previously.

282

### 283 *Neural representations of context-dependent behavioral updating*

284           Also advancing beyond previous work, we identified neural activity predictive of  
285 context-dependent behavioral updates in DLPFC and across the frontal cortex. In the high-noise  
286 condition, small errors provided ambiguous feedback that could reflect either a change in state or  
287 environmental noise. Accordingly, after small errors in the high-noise condition, participants  
288 exhibited variability across trials in whether they switched from their current choice on the  
289 subsequent trial or not. In these ambiguous situations, the multivariate neural pattern across  
290 frontal regions, including OFC, ACC, DMFC and DLPFC, predicted whether people switched or  
291 stayed on the subsequent trial. That is, the multivariate pattern in frontal regions could  
292 distinguish whether people would update their behavior or not in response to the same exact  
293 error stimuli. These results suggest a dissociation between PPC regions that monitor error  
294 information in a context-dependent manner and frontal regions that may use this information to  
295 update beliefs and select subsequent actions.

296           This ability to decode subsequent choices might arise from different kinds of  
297 representations in different areas of frontal cortex. Activity in DMFC reflects the extent of belief  
298 updating in dynamic environments (Behrens et al., 2007; Hampton, Bossaerts, & O'Doherty,  
299 2006; McGuire et al., 2014; O'Reilly et al., 2013), and the multivariate pattern in this region can  
300 decode subsequent switching versus staying in a reversal learning task (Hampton & O'Doherty,  
301 2007). OFC and DMFC encode the identity of the current latent state in a mental model of the  
302 task environment and neural representations in these regions changes as the state changes (Chan,  
303 Niv, & Norman, 2016; Hunt et al., 2018; Karlsson, Tervo, & Karpova, 2012; Nassar, McGuire,  
304 et al., 2019; Schuck, Cai, Wilson, & Niv, 2016; Wilson, Takahashi, Schoenbaum, & Niv, 2014).

305 Neural activity in frontopolar cortex (Daw, O'Doherty, Dayan, Seymour, & Dolan, 2006) and  
306 DMFC (Blanchard & Gershman, 2018; Kolling, Behrens, Mars, & Rushworth, 2012; Kolling et  
307 al., 2016; Muller, Mars, Behrens, & O'Reilly, 2019) increases during exploratory choices, which  
308 occur more frequently during periods of uncertainty about the most beneficial option. In a recent  
309 study, we identified distinct representations of latent states, uncertainty, and behavioral policy in  
310 distinct areas of frontal cortex during learning in a dynamic environment (Nassar et al., 2019).  
311 Our results extend these past findings and demonstrate the role of these frontal regions in  
312 adjusting behavior in response to ambiguous errors.

313

### 314 *Conclusion*

315 People adapt their behavior in response to errors in a context-dependent manner,  
316 distinguishing between errors that indicate change-points in the environment versus noise. Here  
317 we used MVPA to identify two distinct kinds of neural signals contributing to these adaptive  
318 behavioral adjustments. In PPC, neural patterns encoded error information in a context-  
319 dependent manner, depending on error magnitude and past errors only under conditions where  
320 these were informative of the source of error. In contrast, activity in frontal cortex could predict  
321 subsequent choices that could be based on this information. These findings suggest a broad  
322 distinction between outcome monitoring in parietal regions and action selection in frontal regions  
323 when learning in dynamic and uncertain environments.

324

## 325 **Materials and Methods**

### 326 *Participants*

327 All procedures were approved by University of Pennsylvania Internal Review Board. We  
328 analyzed data from sixteen participants (9 female, mean age = 23.5, SD = 4.3, range = 18–33  
329 years) recruited for the current study. One additional participant was excluded from analyses  
330 because of large head movements during MRI scanning (>10% of timepoint-to-timepoint  
331 displacements were >0.5 mm). All participants provided informed consent before the experiment.  
332 Participants received a participation fee of \$15, as well as extra incentives based on their  
333 performance (mean = \$15.09, SD = \$2.26, range = \$8.5–17.5).

334

### 335 *Task*

336 Participants performed a predictive-inference task during MRI scanning. On each trial,  
337 participants saw a noisy observation sampled from an unobserved state. The participants' goal  
338 was to predict the location of the noisy observation. To perform this task well, however, they  
339 should infer the location of the current state.

340 In this task (Li et al., 2019), there were 10 targets aligned in a circle on the screen (Figure  
341 1A). At the start of each trial, participants had to fixate a central cross for 0.5 seconds to  
342 initialize the trial. After the cross disappeared, participants could choose one of 10 targets (red)  
343 by looking at it within 1.5 seconds and keeping fixation on the chosen target for 0.3 seconds.  
344 Then, an outcome would be shown for 1 second. During the outcome phase, a green dot  
345 indicated the chosen target. A purple or cyan target indicated the rewarded target, with color  
346 denoting 10 or 20 points of reward value, respectively. At the end of experiment, every 75 points  
347 were converted to \$0.25 as participants' extra incentives.

348 Participants performed this task in two dynamic conditions separated into two different  
349 runs: a high-noise condition and an unstable condition. In the high-noise condition, the rewarded  
350 target could be one of five targets, given the underlying state (Figure 1B). The rewarded target  
351 probabilities for the relative locations ( $[-2, -1, 0, 1, 2]$ ) of the current state were  $[0.05, 0.15, 0.6,$   
352  $0.15, 0.05]$ . Thus, the location of the current state was most likely rewarded, but nearby targets  
353 could also be rewarded. Occasionally, the state would change its location with a hazard rate of  
354 0.02 (Figure 1C). When a change-point happens, the new state would be selected among the ten  
355 targets based on a uniform distribution. In the unstable condition, there was no noise (Figure 1D).  
356 That is, the location of the state would be always rewarded. However, the state was unstable, as  
357 the hazard rate in this condition was 0.35 (Figure 1E). There were 300 trials in each run.

### 358 359 *Behavior analysis*

360 We investigated how participants' used error feedback flexibly across different contexts.  
361 Before the behavioral analysis, we removed two different kinds of trials. First, we removed trials  
362 in which participants did not make a choice within the time limit (Unstable: median number of  
363 trials = 10.5, range = 1–83; High-noise: median = 10, range = 2–88). Second, we also removed  
364 trials in which the location of the chosen target was not on the shortest distance between the  
365 previously chosen and previously rewarded targets (Unstable: median = 3, range = 0–24; High-  
366 noise: median = 17, range = 5–37). These trials implied that participants might have lost track of

367 the most recently rewarded target and cannot be captured by any of the belief updating models  
368 we tested.

369 First, we investigated how fast participants learned the location of the current state. For  
370 each condition and participant, we binned trials from trial 0 to trial 20 after change-points. Then,  
371 we calculated the probability of choosing the location of the current state for each bin.

372 Second, we examined how different magnitudes of errors lead to shifts in behavior. For  
373 each condition and participant, we binned trials based on the current error magnitude (from 0 to  
374 5). Then, for each bin, we calculated the probability that participants switch their choice to  
375 another target on the subsequent trial. We hypothesized participants would have a lower  
376 probability of switching after small error magnitudes (1 or 2) in the high-noise condition than in  
377 the unstable condition since such errors could be due to environment noise in the high-noise  
378 condition but would signal a state change in the unstable condition.

379 Third, we further investigated how error history influenced participants' behavioral shifts.  
380 Similarly, we binned trials based on the current error magnitude and the error history of the last  
381 three trials. Here, we used four bins of error magnitudes (0, 1, 2, 3+). Based on the outcome of  
382 correct or error on the last three trials, there were 8 types of error history. For each error  
383 magnitude, we calculated the probability of switching for each type of error history. We  
384 hypothesized that participants in the high-noise condition would tend to switch their choice after  
385 small errors more if they had made more errors recently. To test this hypothesis, we ordered the  
386 8 types of error history based on the number of recent errors and calculated the slope of  
387 probability of switching against the order of error history. A negative slope means that  
388 participants tend to switch as they receive more recent errors.

389

### 390 *Behavior modeling*

391 We fit several different computational models to participants' choices to evaluate which  
392 ones could best account for their behavior in the task.

393

### 394 *Reduced Bayesian (RB) model*

395 Previous studies have shown that a reduced Bayesian model, which approximates the full  
396 Bayesian ideal observer, could account well for participants' behavior in dynamic environments

397 similar to the current task (McGuire et al., 2014; Nassar et al., 2012; Nassar et al., 2010). In this  
398 model, belief is updated by a delta rule:

399

$$400 \quad \delta_t = x_t - B_t \quad (1)$$

$$401 \quad B_{t+1} = B_t + \alpha_t \delta_t \quad (2)$$

402

403 where  $B_t$  is the current belief and  $x_t$  is the current observation. The new belief ( $B_{t+1}$ ) is formed  
404 by updating the old belief according to the prediction error ( $x_t - B_t$ ) and a learning rate ( $\alpha_t$ ).

405 The learning rate controls how much a participant revises their belief based on the prediction  
406 error. In this model, the learning rate is adjusted on a trial-by-trial basis according to:

407

$$408 \quad \alpha_t = \Omega_t + (1 - \Omega_t)\tau_t \quad (3)$$

409

410 where  $\Omega_t$  is the change-point probability and  $\tau_t$  is the relative uncertainty. That is,  $\alpha_t$  is high as  
411 either  $\Omega_t$  or  $\tau_t$  is high. The change-point probability is the relative likelihood that the new  
412 observation represents a change-point as opposed to a sample from the currently inferred state  
413 (Nassar et al., 2010):

414

$$415 \quad \Omega_t = \frac{U(x_t|1, 10)^H}{U(x_t|1, 10)^H + f_p(x_t|\gamma_t, B_t)^{(1-H)}} \quad (4)$$

416

417 where  $H$  is the hazard rate,  $U(x_t|1, 10)$  is the probability of outcome derived from a uniform  
418 distribution, and  $f_p(x_t|\gamma_t, B_t)$  is the probability of outcome derived from the current predictive  
419 distribution. That is,  $U(x_t|1, 10)$  reflects the probability of outcome when a change-point has  
420 occurred while  $f_p(x_t|\gamma_t, B_t)$  reflects the probability of outcome when the state has not changed.

421 The predictive distribution is an integration of the state distribution and the noise distribution:

422

$$423 \quad f_p(X|\gamma_t, B_t) = C \times P(X|B_t)^{\gamma_t} \times P(X|B_t) \quad (5)$$

424

425 where  $X$  is a random variable determining the locations of target,  $P(X|B_t)$  is the noise  
426 distribution in the current condition,  $P(X|B_t)^{\gamma_t}$  is the state distribution,  $\gamma_t$  is the expected run

427 length after the change-point, and  $C$  is a normalizing constant to make the sum of probabilities in  
428 the predictive distribution equal one. Thus, the uncertainty of this predictive distribution comes  
429 from two sources: the uncertainty of the state distribution ( $\sigma_s^2$ ) and the uncertainty of the noise  
430 distribution ( $\sigma_N^2$ ). The uncertainty of the state distribution would decrease as the expected run  
431 length increases.

432 The expected run length reflects the expected number of trials that a state remains stable,  
433 and thus is updated on each trial based on the change-point probability (Nassar et al., 2010):

$$434 \gamma_{t+1} = (\gamma_t + 1)(1 - \Omega_t) + \Omega_t \quad (6)$$

436 where the expected run length is a weighted average conditional on the change-point probability.  
437 If no change-point occurs (i.e., change-point probability is low), the expected run length would  
438 increase, leading the uncertainty of the state distribution to decrease. That is, as more  
439 observations from the current state are received, participants are more certain about the location  
440 of the current state. However, if the change-point probability is high, which signals a likely  
441 change in the state, the expected run length would be reset to 1. Thus, the uncertainty of the state  
442 distribution becomes large. Participants are more uncertain about the current state after a change-  
443 point.

444 The other factor influencing the learning rate is the relative uncertainty, which is the  
445 uncertainty regarding the current state relative to the irreducible uncertainty or noise (McGuire et  
446 al., 2014; Nassar et al., 2012):

$$447 \tau_{t+1} = \frac{\Omega_t \sigma_N^2 + (1 - \Omega_t) \sigma_s^2 + \Omega_t (1 - \Omega_t) [\delta_t (1 - \tau_t)]^2}{\Omega_t \sigma_N^2 + (1 - \Omega_t) \sigma_s^2 + \Omega_t (1 - \Omega_t) [\delta_t (1 - \tau_t)]^2 + \sigma_N^2} \quad (7)$$

448 The three terms in the numerator contribute to the uncertainty about the current state. The first  
449 term reflects the uncertainty conditional on the change-point distribution; the second term  
450 reflects the uncertainty conditional on the non-change-point distribution; and the third term  
451 reflects the uncertainty due to the difference between the two distributions. The denominator  
452 shows the total variance which is the summation of the uncertainty about the current state and the



456 noise. As more precise observations are received in a given state, this relative uncertainty would  
457 decrease.

458 During model fitting, the noise distribution was approximated by the von Mises  
459 distribution, which is a circular Gaussian distribution:

460

$$461 \quad P(x_t|B_t, K) = \frac{e^{K \cos(x_t - B_t)}}{\sum_{i=1}^{10} e^{K \cos(x_i - B_t)}} \quad (8)$$

462

463 where  $B_t$  is the location of the current belief,  $x_i$  is the location of target, and  $K$  controls the  
464 uncertainty of this distribution. When  $K$  is 0, this is a uniform distribution. As  $K$  increases, the  
465 uncertainty decreases. The denominator is used as a normalization term to make sure the sum of  
466 all the probabilities equals one. Thus, there are two free parameters in this model: hazard rate ( $H$ )  
467 and noise level ( $K$ ). The range of hazard rate is between 0 and 1 and the noise level is greater  
468 than or equal to zero.

469

470 Fixed learning rate (fixedLR) model

471 We also consider an alternative model in which participants used a fixed learning rate in  
472 each of the two dynamic conditions. That is, the learning rate is the same over all trials in a  
473 condition. This model has one free parameter, the fixed learning rate ( $\alpha_{fixed}$ ), for each condition  
474 (Eq. 2). The fixed learning rate is between 0 and 1.

475

476 Hybrid of RB model and fixedLR model

477 Furthermore, we consider a hybrid model, in which the learning rate on each trial is a  
478 mixture of the learning rates from the RB model and the fixedLR model:

479

$$480 \quad \alpha_t = w\alpha_{RB} + (1 - w)\alpha_{fixed} \quad (9)$$

481

482 where  $\alpha_{RB}$  is the learning rate from the RB model and is varied trial by trial according to  $\Omega_t$  and  
483  $\tau_t$ ,  $\alpha_{fixed}$  is the learning rate from the fixedLR model and  $w$  reflects the weight to integrate these  
484 two learning rates. In this model, there are four free parameters: hazard rate, noise level, fixed  
485 learning rate and weight. The weight is between 0 and 1.

486

487 Hybrid of RB model and  $P_{stay}$

488 Finally, we consider a hybrid model, which combines the RB model with a fixed  
489 tendency to stay on the current target regardless of the current observation. Such a fixed  
490 tendency to stay was observed in monkeys in our previous study (Li et al., 2019). Here the belief  
491 is updated by:

492

493 
$$B_{t+1} = B_t + [(1 - P_{stay}) \times \alpha_t (X_t - B_t) + P_{stay} \times 0] \quad (10)$$

494

495 where  $P_{stay}$  is the probability that participants stay on the current target. This model has three  
496 free parameters: hazard rate, noise level and the probability of stay. The probability of stay is  
497 between 0 and 1.

498

499 Model fitting and comparison

500 Each model was fitted within each participant and within each condition separately.  
501 Optimal parameters were estimated by minimizing the mean of the squared error (MSE) between  
502 a participant's prediction and the model prediction.

503

504 
$$MSE = \frac{\sum_{t=1}^n (B_t - \widehat{B}_t)^2}{n} \quad (11)$$

505

506 where  $t$  is the trial,  $n$  is the total number of included trials,  $B_t$  is a participant's prediction on trial  
507  $t$ , and  $\widehat{B}_t$  is the model prediction on trial  $t$ .

508 Since each model used a different number of parameters and each participant had a  
509 different number of included trials, we used Bayesian Information Criterion (BIC) to compare  
510 the performance of different models:

511

512 
$$BIC = n \ln(MSE) + k \ln(n) \quad (12)$$

513

514 where  $n$  is the number of included trials and  $k$  is the number of free parameters in a model. A  
515 model with lower BIC performs better.

516

517 *MRI Data Acquisition and Preprocessing*

518 We acquired MRI data on a 3T Siemens Prisma with a 64-channel head coil. Before the  
519 task, we acquired a T1-weighted MPRAGE structural image (0.9375 X 0.9375 X 1 mm voxels,  
520 192 X 256 matrix, 160 axial slices, TI = 1,100 ms, TR = 1,810 ms, TE = 3.45 ms, flip angle = 9°).  
521 During each run of the task, we acquired functional data using a multiband gradient echo-planar  
522 imaging (EPI) sequence (1.9592 X 1.9592 X 2 mm voxels, 98 X 98 matrix, 72 axial slices tilted  
523 30° from the AC-PC plane, TR = 1,500 ms, TE = 30 ms, flip angle = 45°, multiband factor = 4).  
524 The scanning time (mean = 24.14 minutes, SD = 1.47, range = 21.85-30.00) for each run was  
525 dependent on the participants' pace. After the task, fieldmap images (TR = 1,270 ms, TE = 5 ms  
526 and 7.46 ms, flip angle = 60°) were acquired.

527 Data were preprocessed using FMRIB's Software Library (FSL) (Jenkinson, Beckmann,  
528 Behrens, Woolrich, & Smith, 2012; Smith et al., 2004). Functional data were motion corrected  
529 using MCFLIRT (Jenkinson, Bannister, Brady, & Smith, 2002), high-pass filtered with a  
530 Gaussian-weighted least square straight line fitting of  $\sigma = 50$  s, undistorted and warped to MNI  
531 space. To map the data to MNI space, boundary-based registration was applied to align the  
532 functional data to the structural image (Greve & Fischl, 2009) and fieldmap-based geometric  
533 undistortion was also applied. In addition, the structural image was normalized to the MNI space  
534 (FLIRT). Then, these two transformations were applied to the functional data.

535

536 *fMRI analysis: univariate activity correlated with CPP and RU*

537 Using similar procedures to our previous study (McGuire et al., 2014), we examined the  
538 effects of CPP and RU on univariate activity. Both the current study and the previous study  
539 investigate the computational process and neural mechanisms during learning in dynamic  
540 environments. The underlying task structures (which involved noisy observations and sudden  
541 change-points) are similar between the two studies, but the two studies used very different visual  
542 stimuli and motor demands. We specifically focused on the high-noise condition in the current  
543 study since it was more similar to the underlying structure, in terms of noisy observations and  
544 hazard rate of change-points, to our previous study.

545 We investigated the factors of CPP, RU, reward values and residual updates. The trial-by-  
546 trial CPP and RU were estimated from the RB model with subjective estimates of hazard rate and

547 noise. The residual update reflects the difference between the participants' update and the  
548 predicted update, and is estimated from a behavioral regression model in a similar manner as our  
549 previous study:

$$550 \quad \text{Update}_t = \beta_0 + \beta_1 \delta_t + \beta_2 \delta_t \Omega_t + \beta_3 \delta_t (1 - \Omega_t) \tau_t + \beta_4 \delta_t \text{Reward} + \varepsilon \quad (13)$$

551  
552 where  $\text{Update}_t$  is the difference between  $B_{t+1}$  and  $B_t$ ,  $\delta_t$  is the error magnitude, both  $\Omega_t$  and  $\tau_t$   
553 were derived from the RB model with subjective estimates of hazard rate and noise, and the  
554 reward value indicated whether a correct response earned a large or a small value on that trial.

555 Then, a general linear model using these four factors was implemented on the neural data.  
556 Here we further smoothed the preprocessed fMRI data with a 6 mm FWHM Gaussian kernel. We  
557 included several trial-by-trial regressors of interest in the GLM: onsets of outcome, CPP, RU,  
558 reward value, and residual update. Six motion parameters were also included as confounds. For  
559 statistical testing, we implemented one-sample cluster-mass permutation tests with 5,000  
560 iterations. The cluster-forming threshold was uncorrected voxel  $p < 0.005$ . Statistical testing was  
561 then based on the corrected cluster  $p$  value. For the conjunction analyses, we used the same  
562 procedure as the previous study (McGuire et al., 2014). We kept regions that passed the  
563 corrected threshold and showed the same sign of effects. For these conjunction tests, we only  
564 kept regions that have at least 10 contiguous voxels.

565 Since the number of participants was fewer in this study ( $n=16$ ) than in the previous  
566 study ( $n=32$ ), we might have lower power to detect effects in the whole-brain analyses. Thus, we  
567 also implemented ROI analyses. We selected seven ROIs that showed the conjunction effects of  
568 CPP, RU and reward value in the previous study (McGuire et al., 2014) and tested the effects of  
569 CPP and RU in these ROIs.

570  
571  
572 *fMRI analysis: multi-voxel pattern analysis (MVPA)*

573 We implemented MVPA to understand the neural representation of error signals and  
574 subsequent choices. Our analyses focus on the multi-voxel pattern when participants received an  
575 outcome. Before implementing MVPA, we estimated trial-by-trial beta values using the  
576 unsmoothed preprocessed fMRI data. We used the general linear model (GLM) to estimate the  
577 beta weights for each trial (Mumford, Turner, Ashby, & Poldrack, 2012). In each GLM, the first

578 regressor is the trial of interest and the second combines the rest of trials in the same condition.  
579 These two regressors were then convolved with a gamma hemodynamic response function. In  
580 addition, six motion parameters were included as control regressors. We repeated this process  
581 (one GLM per trial) to estimate trial-by-trial beta values for all the trials in the two conditions.  
582 We then used these beta values as observations for MVPA. A whole-brain searchlight was  
583 implemented (Kriegeskorte, Goebel, & Bandettini, 2006). In each searchlight, a sphere with the  
584 diameter of 5 voxels (10 mm) was formed, and the pattern of activity across the voxels within the  
585 sphere were used to run MVPA.

586 A support vector machine (SVM) with a linear kernel was used to decode different error  
587 signals and choices in our whole-brain searchlight analysis. We implemented SVM through the  
588 LIBSVM toolbox (Chang & Lin, 2011). To avoid overfitting, we used 3-fold cross-validation,  
589 with one fold used as testing data and the other two as training data. Training data were used to  
590 train the classifier and then this classifier was used on testing data to examine the classification  
591 accuracy. In linear SVM, a free parameter  $c$  regularizes the trade-off between decreasing training  
592 error and increasing generalization. Thus, during the training of classifier, the training data were  
593 further split into 3-folds to select the optimal value of the parameter  $c$  through cross-validation.  
594 We pick the optimal value for  $c$  from [0.001, 0.01, 0.1, 1, 10, 100, 1000] and this optimal  
595 parameter should maximize the cross-validation accuracy. Then, we used the optimal parameter  
596  $c$  to train the model again based on the entire training data and calculated the classification  
597 accuracy on the testing data. We repeated this procedure with each of the three folds held out as  
598 testing data and calculated the average of the classification accuracy. To minimized the influence  
599 of different number of trials for each category on the classification accuracy, we used balanced  
600 accuracy.

601 We first examined how the multi-voxel neural pattern on the current trial could  
602 discriminate correct versus error on the current trial or error magnitudes on the current error trial.  
603 For the analysis of correct versus error, the baseline accuracy is 50%. For the analysis of error  
604 magnitudes, we split trials into three bins of error magnitude: 1, 2, and 3+. Thus, the baseline  
605 accuracy is 33%.

606 We next examined how the multi-voxel neural pattern on the current trial could  
607 discriminate whether the previous trial was an error or not. We also investigated how the  
608 classification of past errors differs conditional on the type of the current trial. We classified trial

609 *t-1* as correct or error separately for four different types of current trials: correct trials, error trials,  
610 unambiguous feedback trials and ambiguous feedback trials. Unambiguous feedback trials were  
611 trials with error magnitudes of 0 or 3+, while ambiguous feedback trials were trials with error  
612 magnitudes of 1 or 2, in which participants would be uncertain about the change of the state in  
613 the high-noise condition.

614 Lastly, we examined how the multi-voxel neural pattern on the current trial could classify  
615 the choice on the next trial. In this analysis, we focused only on the trials with error magnitudes  
616 of 1 or 2 in the high-noise condition, since only under these conditions were participants  
617 similarly likely to switch versus stay. For these trials, we examined whether the multi-voxel  
618 pattern on the current trial predicted whether the participant stayed or switched on the next trial.  
619 The baseline accuracy was 50%.

620 After obtaining the classification accuracy for each participant, we subtracted the baseline  
621 accuracy from the classification accuracy. Before conducting a group-level test, we smoothed  
622 these individual accuracy maps with a 6 mm FWHM Gaussian kernel. For statistical testing, one-  
623 sample cluster-mass permutation was applied with 5,000 iterations. We used uncorrected voxel  
624  $p < 0.005$  to form a cluster and estimated the corrected cluster  $p$  value for each cluster. For the  
625 conjunction analyses, we used the same procedure described above.

626

627 **Acknowledgments**

628 This work was supported by grants from National Institute of Mental Health (R01-MH098899 to  
629 J.I.G. and J.W.K.) and National Science Foundation (1533623 to J.I.G. and J.W.K.). We thank  
630 Yin Li for valuable comments; M. Kathleen Caulfield for fMRI scanning.

631

632 **Competing interests**

633 The authors declare no competing interests.

634

635

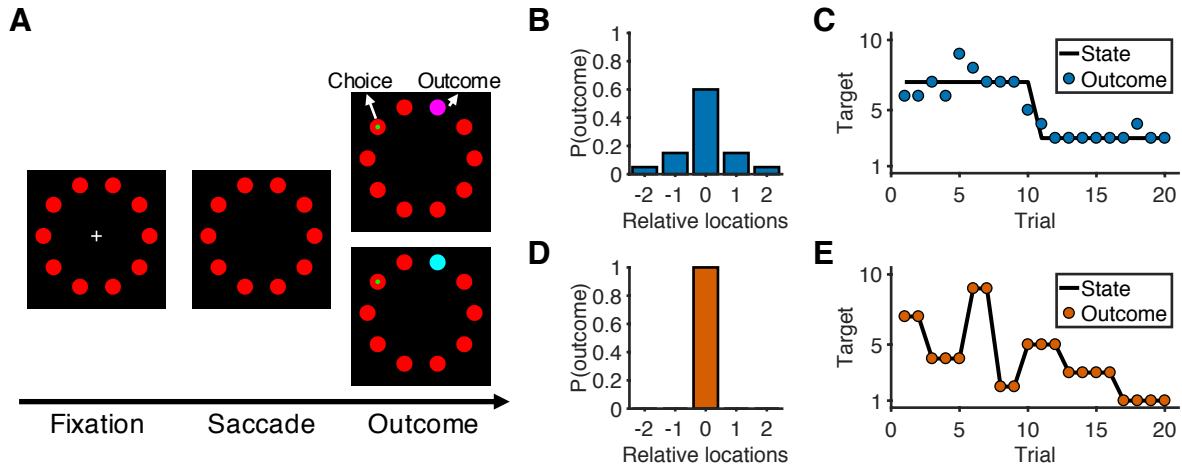
## References

- 636 Akrami, A., Kopec, C. D., Diamond, M. E., & Brody, C. D. (2018). Posterior parietal cortex  
637 represents sensory history and mediates its effects on behaviour. *Nature*, *554*, 368.  
638 doi:10.1038/nature25510
- 639 Behrens, T. E. J., Woolrich, M. W., Walton, M. E., & Rushworth, M. F. S. (2007). Learning the  
640 value of information in an uncertain world. *Nat Neurosci*, *10*(9), 1214-1221.  
641 doi:10.1038/nn1954
- 642 Blanchard, T. C., & Gershman, S. J. (2018). Pure correlates of exploration and exploitation in the  
643 human brain. *Cognitive, Affective, & Behavioral Neuroscience*, *18*(1), 117-126.  
644 doi:10.3758/s13415-017-0556-2
- 645 Brody, C. D., & Hanks, T. D. (2016). Neural underpinnings of the evidence accumulator.  
646 *Current Opinion in Neurobiology*, *37*, 149-157. doi:10.1016/j.conb.2016.01.003
- 647 Chan, S. C. Y., Niv, Y., & Norman, K. A. (2016). A Probability Distribution over Latent Causes,  
648 in the Orbitofrontal Cortex. *The Journal of Neuroscience*, *36*(30), 7817-7828.  
649 doi:10.1523/jneurosci.0659-16.2016
- 650 Chang, C.-C., & Lin, C.-J. (2011). LIBSVM: a library for support vector machines. *ACM*  
651 *transactions on intelligent systems and technology*, *2*(3), 27.  
652 doi:10.1145/1961189.1961199
- 653 d'Acromont, M., & Bossaerts, P. (2016). Neural Mechanisms Behind Identification of  
654 Leptokurtic Noise and Adaptive Behavioral Response. *Cerebral Cortex*, *26*(4), 1818-  
655 1830. doi:10.1093/cercor/bhw013
- 656 Daw, N. D., O'Doherty, J. P., Dayan, P., Seymour, B., & Dolan, R. J. (2006). Cortical substrates  
657 for exploratory decisions in humans. *Nature*, *441*(7095), 876-879.  
658 doi:10.1038/nature04766
- 659 Fischer, Adrian G., & Ullsperger, M. (2013). Real and Fictive Outcomes Are Processed  
660 Differently but Converge on a Common Adaptive Mechanism. *Neuron*, *79*(6), 1243-  
661 1255. doi:10.1016/j.neuron.2013.07.006
- 662 FitzGerald, T. H. B., Moran, R. J., Friston, K. J., & Dolan, R. J. (2015). Precision and neuronal  
663 dynamics in the human posterior parietal cortex during evidence accumulation.  
664 *NeuroImage*, *107*, 219-228. doi:10.1016/j.neuroimage.2014.12.015
- 665 Furl, N., & Averbeck, B. B. (2011). Parietal Cortex and Insula Relate to Evidence Seeking  
666 Relevant to Reward-Related Decisions. *The Journal of Neuroscience*, *31*(48), 17572-  
667 17582. doi:10.1523/jneurosci.4236-11.2011
- 668 Gläscher, J., Daw, N., Dayan, P., & O'Doherty, J. P. (2010). States versus Rewards: Dissociable  
669 Neural Prediction Error Signals Underlying Model-Based and Model-Free Reinforcement  
670 Learning. *Neuron*, *66*(4), 585-595. doi:10.1016/j.neuron.2010.04.016
- 671 Glaze, C. M., Kable, J. W., & Gold, J. I. (2015). Normative evidence accumulation in  
672 unpredictable environments. *eLife*, *4*, e08825. doi:10.7554/eLife.08825
- 673 Greve, D. N., & Fischl, B. (2009). Accurate and robust brain image alignment using boundary-  
674 based registration. *NeuroImage*, *48*(1), 63-72. doi:10.1016/j.neuroimage.2009.06.060
- 675 Hampton, A. N., Bossaerts, P., & O'Doherty, J. P. (2006). The Role of the Ventromedial  
676 Prefrontal Cortex in Abstract State-Based Inference during Decision Making in Humans.  
677 *The Journal of Neuroscience*, *26*(32), 8360-8367. doi:10.1523/jneurosci.1010-06.2006
- 678 Hampton, A. N., & O'Doherty, J. P. (2007). Decoding the neural substrates of reward-related  
679 decision making with functional MRI. *Proceedings of the National Academy of Sciences*,  
680 *104*(4), 1377-1382. doi:10.1073/pnas.0606297104



- 681 Hanks, T. D., Kopec, C. D., Brunton, B. W., Duan, C. A., Erlich, J. C., & Brody, C. D. (2015).  
682 Distinct relationships of parietal and prefrontal cortices to evidence accumulation.  
683 *Nature*, 520, 220. doi:10.1038/nature14066
- 684 Hayden, B. Y., Nair, A. C., McCoy, A. N., & Platt, M. L. (2008). Posterior Cingulate Cortex  
685 Mediates Outcome-Contingent Allocation of Behavior. *Neuron*, 60(1), 19-25.  
686 doi:10.1016/j.neuron.2008.09.012
- 687 Hunt, L. T., Malalasekera, W. M. N., de Berker, A. O., Miranda, B., Farmer, S. F., Behrens, T.  
688 E. J., & Kennerley, S. W. (2018). Triple dissociation of attention and decision  
689 computations across prefrontal cortex. *Nature Neuroscience*, 21(10), 1471-1481.  
690 doi:10.1038/s41593-018-0239-5
- 691 Hwang, E. J., Dahlen, J. E., Mukundan, M., & Komiyama, T. (2017). History-based action  
692 selection bias in posterior parietal cortex. *Nature Communications*, 8(1), 1242.  
693 doi:10.1038/s41467-017-01356-z
- 694 Jenkinson, M., Bannister, P., Brady, M., & Smith, S. (2002). Improved Optimization for the  
695 Robust and Accurate Linear Registration and Motion Correction of Brain Images.  
696 *NeuroImage*, 17(2), 825-841. doi:10.1006/ning.2002.1132
- 697 Jenkinson, M., Beckmann, C. F., Behrens, T. E., Woolrich, M. W., & Smith, S. M. (2012). FSL.  
698 *NeuroImage*, 62(2), 782-790. doi:10.1016/j.neuroimage.2011.09.015
- 699 Karlsson, M. P., Tervo, D. G. R., & Karpova, A. Y. (2012). Network Resets in Medial Prefrontal  
700 Cortex Mark the Onset of Behavioral Uncertainty. *Science*, 338(6103), 135-139.  
701 doi:10.1126/science.1226518
- 702 Kolling, N., Behrens, T. E. J., Mars, R. B., & Rushworth, M. F. S. (2012). Neural Mechanisms of  
703 Foraging. *Science*, 336(6077), 95-98. doi:10.1126/science.1216930
- 704 Kolling, N., Wittmann, M. K., Behrens, T. E. J., Boorman, E. D., Mars, R. B., & Rushworth, M.  
705 F. S. (2016). Value, search, persistence and model updating in anterior cingulate cortex.  
706 *Nature Neuroscience*, 19, 1280. doi:10.1038/nn.4382
- 707 Kriegeskorte, N., Goebel, R., & Bandettini, P. (2006). Information-based functional brain  
708 mapping. *Proceedings of the National Academy of Sciences of the United States of*  
709 *America*, 103(10), 3863-3868. doi:10.1073/pnas.0600244103
- 710 Li, Y. S., Nassar, M. R., Kable, J. W., & Gold, J. I. (2019). Individual neurons in the cingulate  
711 cortex encode action monitoring, not selection, during adaptive decision-making. *The*  
712 *Journal of Neuroscience*, 0159-0119. doi:10.1523/jneurosci.0159-19.2019
- 713 McGuire, J. T., Nassar, M. R., Gold, J. I., & Kable, J. W. (2014). Functionally Dissociable  
714 Influences on Learning Rate in a Dynamic Environment. *Neuron*, 84(4), 870-881.  
715 doi:10.1016/j.neuron.2014.10.013
- 716 Muller, T. H., Mars, R. B., Behrens, T. E., & O'Reilly, J. X. (2019). Control of entropy in neural  
717 models of environmental state. *eLife*, 8, e39404. doi:10.7554/eLife.39404
- 718 Mumford, J. A., Turner, B. O., Ashby, F. G., & Poldrack, R. A. (2012). Deconvolving BOLD  
719 activation in event-related designs for multivoxel pattern classification analyses.  
720 *NeuroImage*, 59(3), 2636-2643. doi:10.1016/j.neuroimage.2011.08.076
- 721 Nassar, M. R., Bruckner, R., & Frank, M. J. (2019). Statistical context dictates the relationship  
722 between feedback-related EEG signals and learning. *eLife*, 8, e46975.  
723 doi:10.7554/eLife.46975
- 724 Nassar, M. R., McGuire, J. T., Ritz, H., & Kable, J. W. (2019). Dissociable Forms of  
725 Uncertainty-Driven Representational Change Across the Human Brain. *The Journal of*  
726 *Neuroscience*, 39(9), 1688-1698. doi:10.1523/jneurosci.1713-18.2018

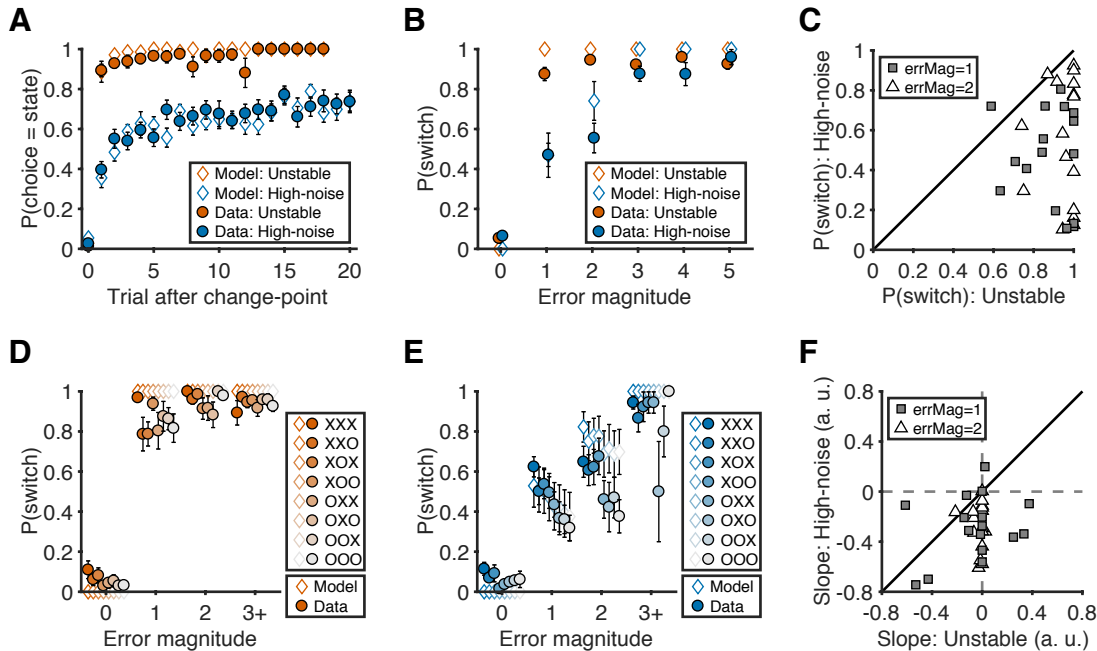
- 727 Nassar, M. R., Rumsey, K. M., Wilson, R. C., Parikh, K., Heasly, B., & Gold, J. I. (2012).  
728 Rational regulation of learning dynamics by pupil-linked arousal systems. *Nature*  
729 *Neuroscience*, *15*(7), 1040-1046. doi:10.1038/nn.3130
- 730 Nassar, M. R., Wilson, R. C., Heasly, B., & Gold, J. I. (2010). An approximately Bayesian delta-  
731 rule model explains the dynamics of belief updating in a changing environment. *The*  
732 *Journal of Neuroscience*, *30*(37), 12366-12378. doi:10.1523/JNEUROSCI.0822-10.2010
- 733 O'Reilly, J. X., Schüffelgen, U., Cuell, S. F., Behrens, T. E. J., Mars, R. B., & Rushworth, M. F.  
734 S. (2013). Dissociable effects of surprise and model update in parietal and anterior  
735 cingulate cortex. *Proceedings of the National Academy of Sciences*, *110*(38), E3660-  
736 E3669. doi:10.1073/pnas.1305373110
- 737 Payzan-LeNestour, E., Dunne, S., Bossaerts, P., & O'Doherty, John P. (2013). The Neural  
738 Representation of Unexpected Uncertainty during Value-Based Decision Making.  
739 *Neuron*, *79*(1), 191-201. doi:10.1016/j.neuron.2013.04.037
- 740 Purcell, B. A., & Kiani, R. (2016). Hierarchical decision processes that operate over distinct  
741 timescales underlie choice and changes in strategy. *Proceedings of the National Academy*  
742 *of Sciences*, *113*(31), E4531-E4540. doi:10.1073/pnas.1524685113
- 743 Schuck, N. W., Cai, M. B., Wilson, R. C., & Niv, Y. (2016). Human Orbitofrontal Cortex  
744 Represents a Cognitive Map of State Space. *Neuron*, *91*(6), 1402-1412.  
745 doi:10.1016/j.neuron.2016.08.019
- 746 Smith, S. M., Jenkinson, M., Woolrich, M. W., Beckmann, C. F., Behrens, T. E., Johansen-Berg,  
747 H., . . . Flitney, D. E. (2004). Advances in functional and structural MR image analysis  
748 and implementation as FSL. *NeuroImage*, *23* (S1), S208-S219.  
749 doi:10.1016/j.neuroimage.2004.07.051
- 750 Sutton, R. S., & Barto, A. G. (1998). *Reinforcement Learning*. Cambridge, MA: MIT Press.
- 751 Wilson, R. C., Takahashi, Y. K., Schoenbaum, G., & Niv, Y. (2014). Orbitofrontal Cortex as a  
752 Cognitive Map of Task Space. *Neuron*, *81*(2), 267-279.  
753 doi:10.1016/j.neuron.2013.11.005  
754  
755



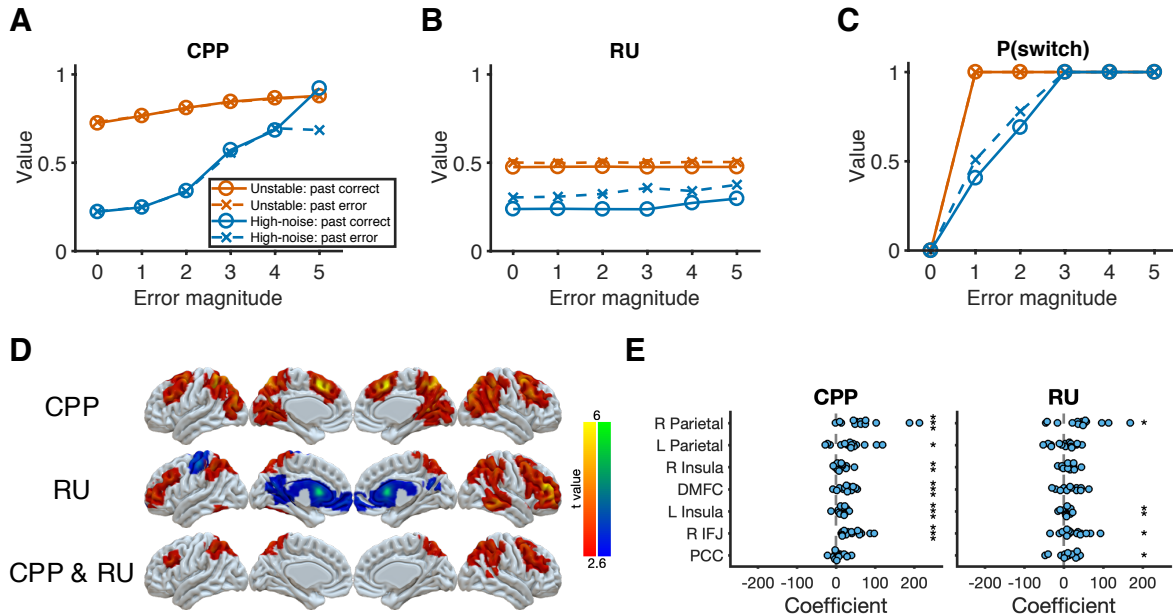
756  
757  
758  
759  
760  
761  
762  
763  
764  
765  
766  
767  
768  
769  
770

**Figure 1**

Overview of task and experimental design. (A) Sequence of the task. At the start of the trial, participants look at a cross in the center of the screen and maintain fixation for 0.5 sec to initialize the trial. After the cross disappears, participants choose one of 10 targets (red) by looking at it within 1.5 sec and then holding fixation on the chosen target for 0.3 sec. During the outcome phase (1 sec), a green dot inside the target indicates the participants' choice. The rewarded target is shown in purple or cyan to indicate the number of earnable points as 10 or 20, respectively. (B) Probability distribution of the rewarded target location in the high-noise condition. Target location is relative to the location of the state (generative mean). The rewarded target probabilities for the relative locations of [-2, -1, 0, 1, 2] are [0.05, 0.15, 0.6, 0.15, 0.05]. (C) Example of trials in the high-noise condition. The states change occasionally with a hazard rate of 0.02. (D) Probability distribution of the rewarded target location in the unstable condition. Because there is no noise in this condition, the rewarded target is always at the location of the state. (E) Example of trials in the unstable condition. The states change frequently with a hazard rate of 0.35.



771  
 772 **Figure 2**  
 773 Behavioral results. (A) Probability of choosing the best target after change-points. Symbols and error bars  
 774 are mean±SEM across subjects (solid symbols) or simulations (open symbols). (B) Relationship between  
 775 error magnitude and switch probability. Symbols and error bars are as in A. (C) The distribution of switch  
 776 probabilities for small errors (magnitude of 1 or 2) in both conditions. Each data point represents one  
 777 participant. (D) Probability of switch as a function of current error magnitude and error history in the  
 778 unstable condition. Different colors represent different error histories for the past 3 trials. A correct trial is  
 779 marked as O, and an error trial is marked as X. For example, XOO implies that trial t-1 was an error trial,  
 780 and trial t-2 and trial t-3 were correct trials. Symbols and error bars are mean±SEM across subjects. (E)  
 781 Probability of switch as a function of current error magnitude and error history in the high-noise condition.  
 782 Symbols and error bars are as in D. (F) The distribution of the slopes of switch probability against error  
 783 history for small errors (magnitude of 1 or 2) in both conditions. Each data point represents one  
 784 participant.  
 785

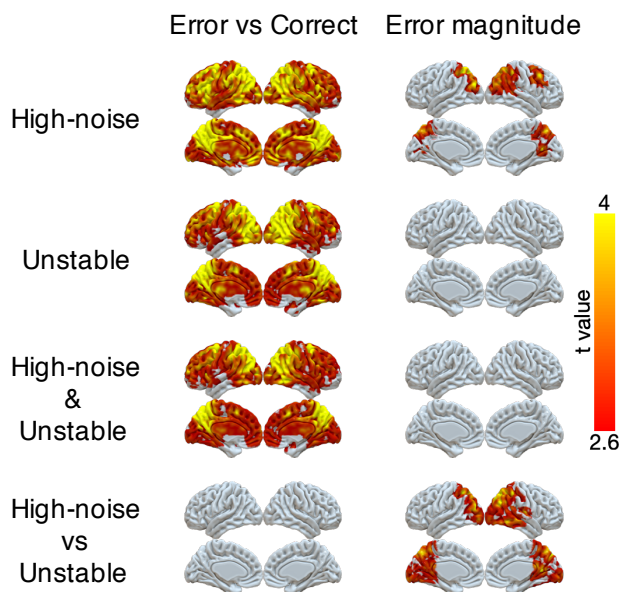


786  
787  
788  
789  
790  
791  
792  
793  
794  
795  
796  
797  
798  
799  
800  
801  
802  
803  
804

**Figure 3**

Reduced Bayesian model applied to behavioral and imaging data. **(A)** Model prediction for CPP. We calculated CPP from the reduced Bayesian model using subjective estimates of hazard rate and noise for each condition. The value of CPP increases as the current error magnitude increases in both conditions, but with a stronger dependence on the outcome of the previous trial in the high-noise condition. **(B)** Model prediction for RU. We calculated RU from the reduced Bayesian model using subjective estimates of hazard rate and noise for each condition. The value of RU is minimally affected by the current error magnitude. Instead, a past error tends to increase RU in the high-noise, but not the unstable, condition. **(C)** Model prediction for probability of switching choices. Increasing CPP causes the probability of switching to increase more steeply as the current error magnitude increases in the unstable condition versus in the high-noise condition. For small errors (error magnitude of 1 and 2) in the high-noise condition, the probability of switching is further influence by RU, which is affected by past errors. **(D)** Neural representation of CPP and RU. **(E)** ROI analysis for CPP and RU. These ROIs were selected based on the common regions of CPP, RU, and reward effects in McGuire et al. (2014). Significance was tested by a sign test. \* $p < 0.05$ , \*\* $p < 0.01$ , \*\*\* $p < 0.001$ .

805



806

**Figure 4**

807

808

809

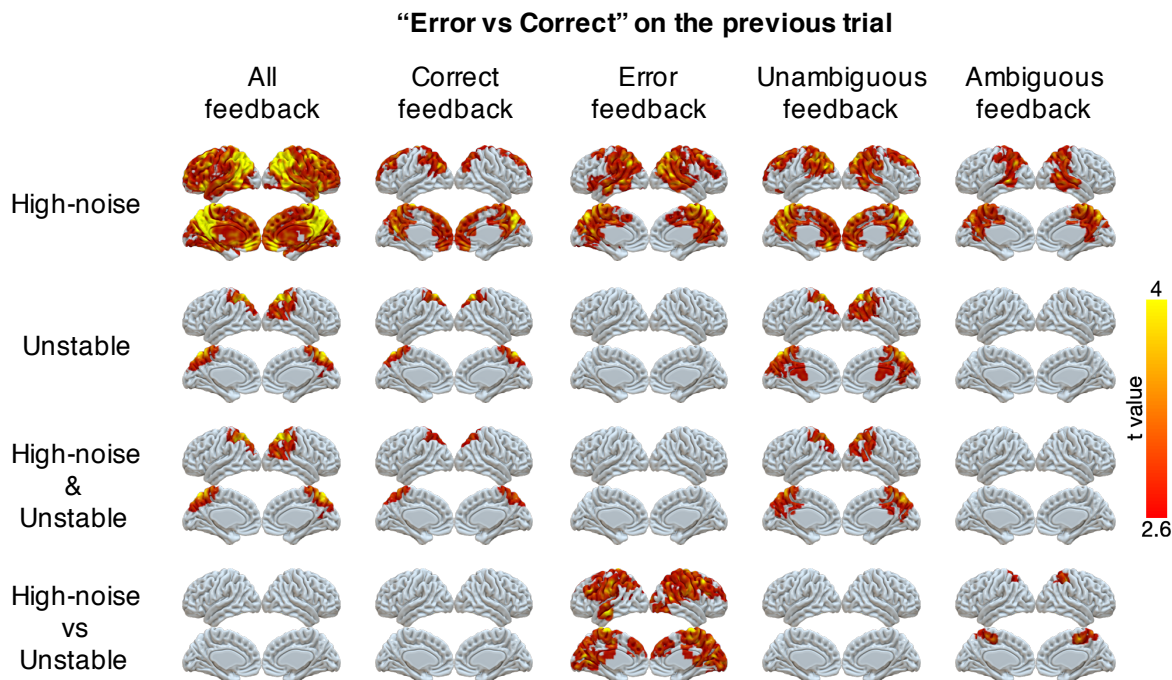
810

811

812

813

Representations of error and error magnitude. For error versus correct analyses, multi-voxel neural patterns were used to classify whether the response on the current trial was correct or an error. For error magnitude analyses, multi-voxel neural patterns were used to classify different error magnitudes (1, 2, 3+) conditional on the current trial being an error. Accuracies were calculated and compared with the baseline accuracy within each subject and then tested at the group level. The representation of current error magnitude is stronger in parietal cortex in the high-noise condition than the unstable condition.

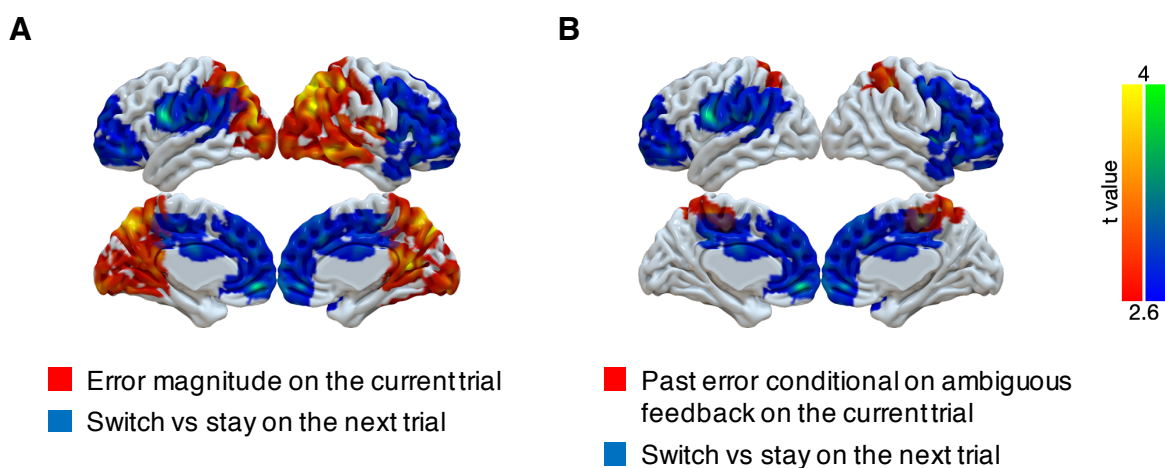


814  
815  
816  
817  
818  
819  
820  
821  
822

**Figure 5**

Representations of errors on the previous trial conditional on different types of current trials (columns). Multi-voxel neural patterns were used to classify correct responses versus errors on the previous trial. This analysis was repeated for different types of current trials: all feedback, correct feedback, error feedback, unambiguous feedback (error magnitudes are 0/3+), and ambiguous feedback (error magnitudes are 1/2). The representation of past errors is stronger in parietal cortex in the high-noise condition than the unstable condition when the current trial is an error or provides ambiguous feedback.

823



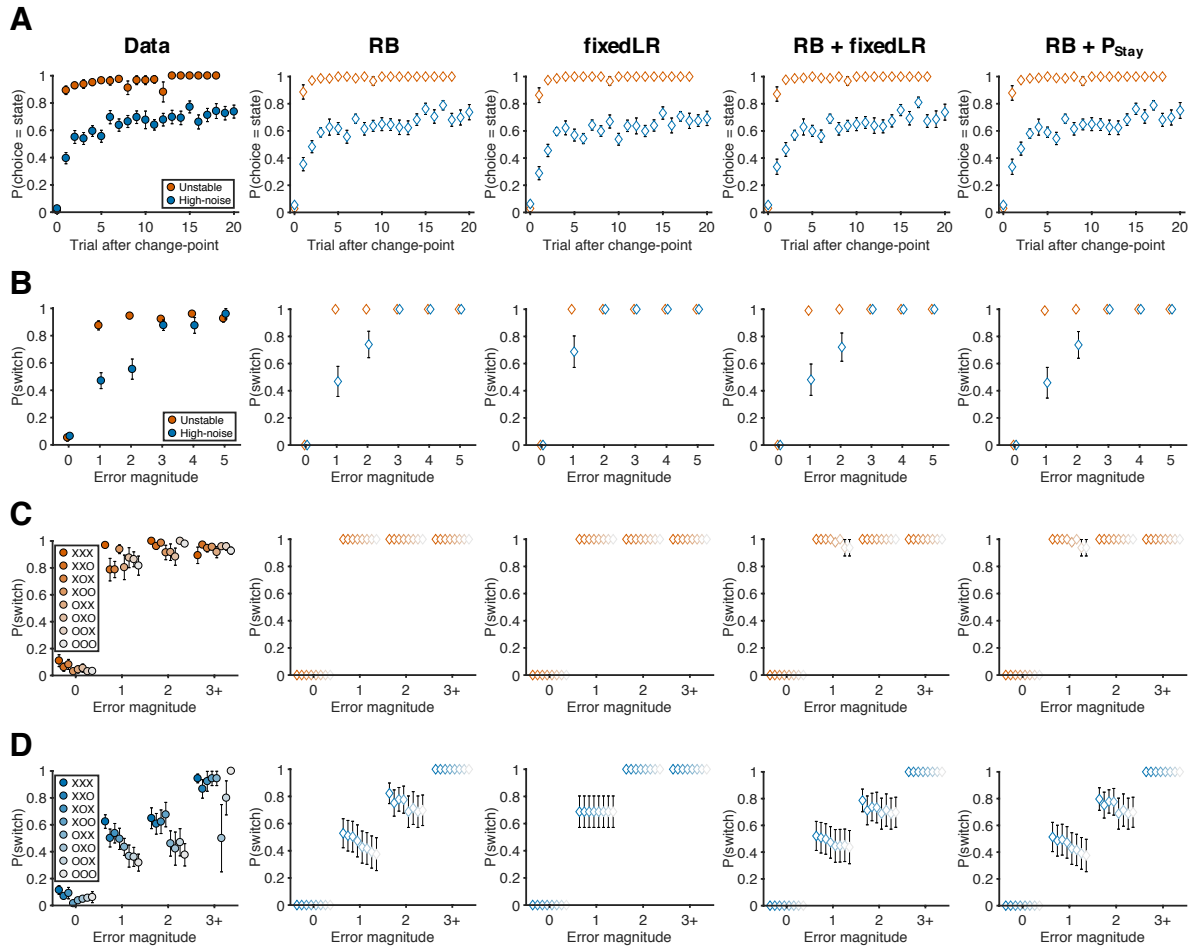
824

825 **Figure 6**

826 Representations of subsequent behavioral choices (switch versus stay) after ambiguous small errors in the  
827 high-noise condition. **(A)** Overlap of results for switch versus stay on the next trial and error magnitude  
828 on the current trial. Multi-voxel neural patterns were used to classify whether participants switch their  
829 choice to another target or stay on the same target on the next trial. We focused on the most ambiguous  
830 errors (error magnitude of 1 or 2 in the high-noise condition). Above-chance classification performance  
831 was found throughout much of the frontal lobe. **(B)** Overlap of results for switch versus stay on the next  
832 trial and past error conditional on ambiguous feedback on the current trial.

833

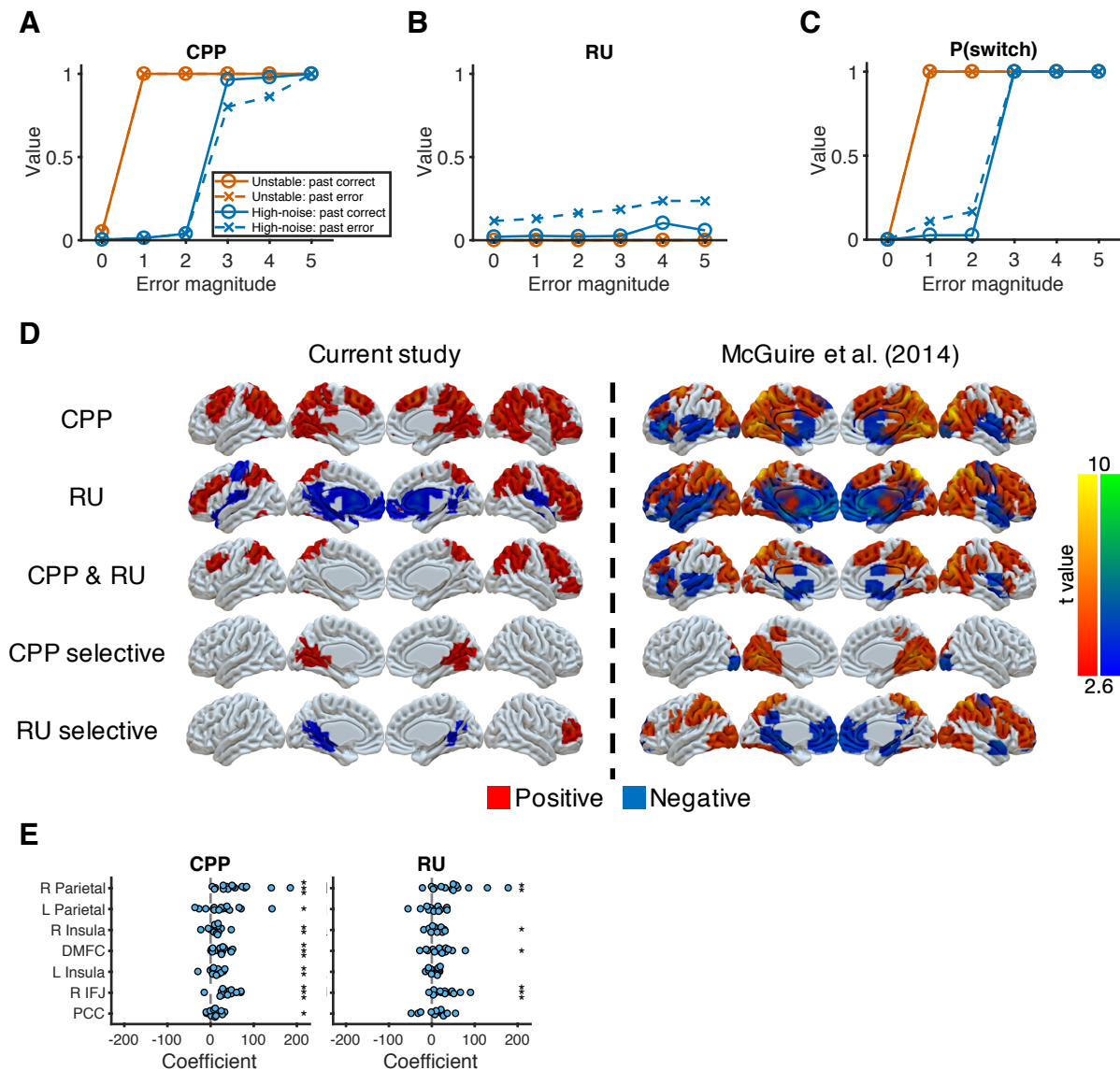




834  
835  
836  
837  
838  
839  
840  
841  
842

**Figure 2 - Figure supplement 1**

Behavioral data and predictions from different models. (A) Probability of choosing the best target after change-points. (RB: reduced Bayesian; fixedLR: fixed learning rate; P<sub>stay</sub>: fixed tendency to stay) (B) The relationship between error magnitude and switch probability. (C) Probability of switch as a function of current error magnitude and error history in the unstable condition. (D) Probability of switch as a function of current error magnitude and error history in the high-noise condition. Symbols and colors are as in Figure 2.



844

845 **Figure 3 - Figure supplement 1**

846 Reduced Bayesian model with true hazard rate and noise applied to behavioral and imaging data. (A)

847 Model prediction for CPP. We calculated CPP from the reduced Bayesian model using the true hazard

848 rate and noise for each condition. (B) Model prediction for RU. We calculated RU from the reduced

849 Bayesian model using the true hazard rate and noise for each condition. (C) Model prediction for

850 probability of switch. Probability of switch is influenced by both CPP and RU. (D) Neural representation

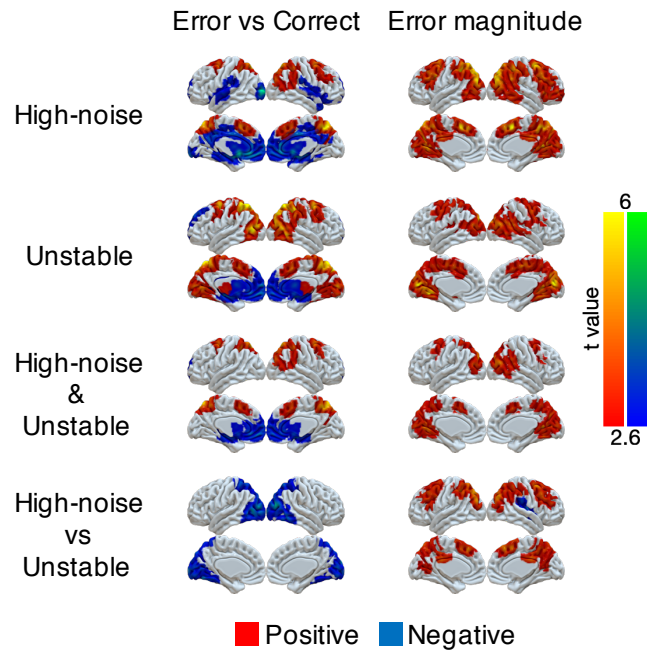
851 of CPP and RU in the current study and in McGuire et al. (2014). CPP selective effect represents the

852 conjunction of CPP&gt;0 and CPP&gt;RU. RU selective effect represents the conjunction of RU&gt;0 and

853 RU&gt;CPP. (E) ROI analysis for CPP and RU. These ROIs were selected based on the common regions of

854 CPP, RU and reward effects in McGuire et al. (2014). Significance was tested by a sign test. \* $p < 0.05$ ,855 \*\* $p < 0.01$ , \*\*\* $p < 0.001$ .

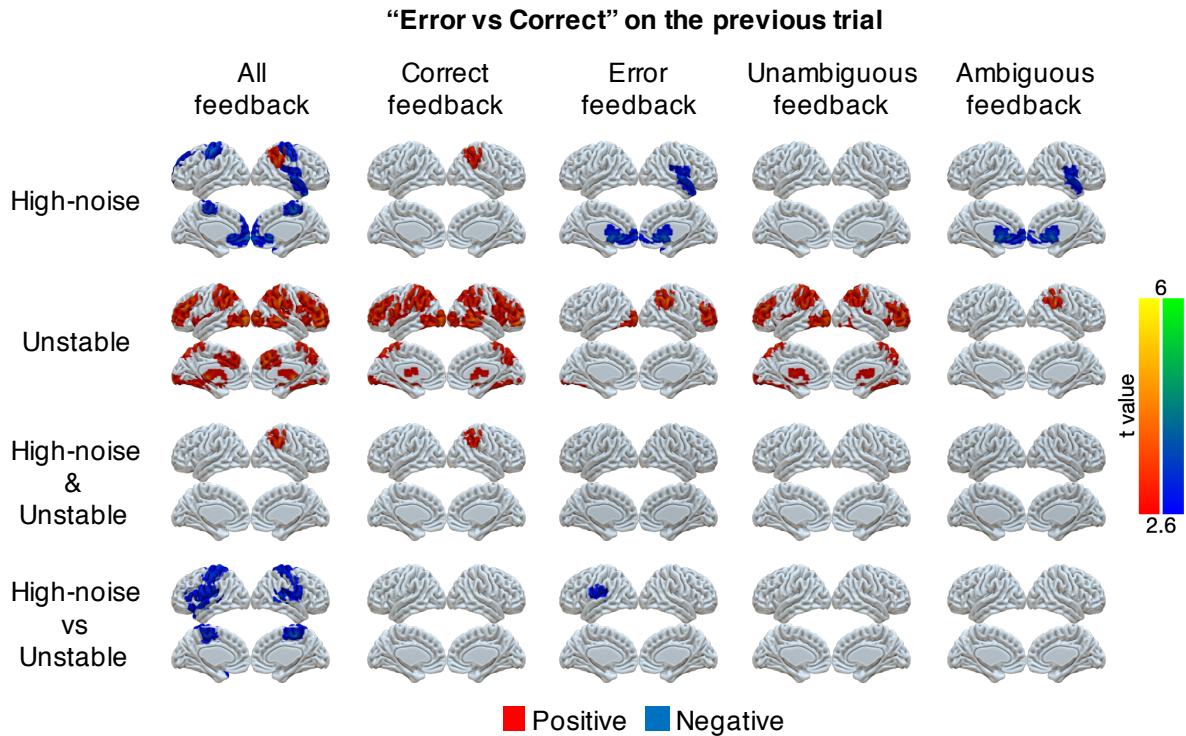
856



858 **Figure 4 - Figure supplement 1**

859 Univariate representations of error and error magnitude. A GLM was implemented on the preprocessed  
 860 fMRI data (smoothed with 6 mm FWHM Gaussian kernel). The trial-by-trial regressors of interest that  
 861 were included in the GLM were: onset of correct trials, earnable value on correct trials, onset of error  
 862 trials, error magnitude on error trials, switch or stay on error trials and earnable value on error trials. We  
 863 focused on the effects of error (which is the difference between the onset of error trials and the onset of  
 864 correct trials) and error magnitude. Group  $t$ -values are shown. For statistical testing, we implemented one-  
 865 sample cluster-mass permutation tests with 5,000 iterations. The cluster-forming threshold was  
 866 uncorrected voxel  $p < 0.005$ .

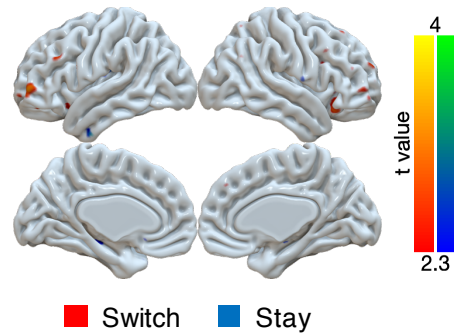
867



868  
869  
870  
871  
872  
873  
874  
875  
876  
877  
878  
879  
880  
881  
882  
883  
884  
885  
886  
887  
888

**Figure 5 - Figure supplement 1**

Univariate representations of error on the previous trial conditional on different types of current trials (columns). Several GLMs were implemented on the preprocessed fMRI data (smoothed with 6 mm FWHM Gaussian kernel). First, we examined errors on the previous trial across all trials. The trial-by-trial regressors of interest that were included in the GLM were: onset of trials, error on trial t, error on trial t-1, error on trial t-2, and error on trial t-3. We focused on the effect of error on trial t-1. Second, we separated the analysis of past errors conditional on the current trial being correct or an error. The trial-by-trial regressors of interest that were included in the GLM were: onset of current correct trials, errors on trial t-1, t-2, or t-3 conditional on the current trial being correct, onset of current error trials, errors on trial t-1, t-2, or t-3 conditional on the current trial being an error. We focused on the effects of error on trial t-1 conditional on the current trial being correct or an error. Third, we separated errors conditional on unambiguous (error magnitudes are 0/3+) or ambiguous feedback (error magnitudes are 1/2). The trial-by-trial regressors of interest that were included in the GLM were: onset of current trials with unambiguous feedback, errors on trial t-1, t-2 or t-3 conditional on the current trial providing unambiguous feedback, onset of current trials with ambiguous feedback, errors on trial t-1, t-2 or t-3 conditional on the current trial providing ambiguous feedback. We focused on the effects of errors on trial t-1 conditional on the current trials providing unambiguous or ambiguous feedback. Group *t*-values are shown. For statistical testing, we implemented one-sample cluster-mass permutation tests with 5,000 iterations. The cluster-forming threshold was uncorrected voxel  $p < 0.005$ .



889  
 890  
 891  
 892  
 893  
 894  
 895  
 896  
 897  
 898  
 899  
 900  
 901  
 902

**Figure 6 - Figure supplement 1**

Univariate GLM for switch versus stay on ambiguous feedback in the high-noise condition. A GLM was implemented with several trial-by-trial regressors of interest: onset of trials with error magnitude of 0, onset of trials with error magnitude of 3+, onset of ambiguous feedback (error magnitudes are 1/2) followed by switching, onset of ambiguous feedback followed by staying. We tested the effects of the difference between switch and stay after ambiguous feedback. Group *t*-values are shown. The results were thresholded based on uncorrected voxel  $p < 0.01$ .

903 Table 1  
 904 BIC of behavior models

Model	Condition	BIC improvement by RB model
Reduced Bayesian model (RB)	Unstable	
	High-noise	
Fixed learning rate model (fixedLR)	Unstable	5.26 [3.97, 5.71]**
	High-noise	-22.22 [-77.36, 0.03] <sup>†</sup>
RB + fixedLR	Unstable	-9.85 [-10.97, -7.65]***
	High-noise	-4.60 [-9.93, 0.98]
RB + P <sub>stay</sub>	Unstable	-5.20 [-5.66, -3.76]**
	High-noise	-5.57 [-5.68, -2.60]**

905 The values were shown as median [IQR]. A negative value means that RB model performed  
 906 better than the compared model. Significance was tested by a sign test. <sup>†</sup> $p < 0.08$ , \*\* $p < 0.01$ ,  
 907 \*\*\* $p < 0.001$ .  
 908

909 Table 2

910 Parameters of behavior models

Model	Parameter	Unstable	High-noise	Unstable > High-noise
RB	H	0.88 [0.68, 0.92]	0.33 [0.11, 0.50]	0.46 [0.25, 0.72]***
	K	0.59 [0.03, 2.22]	1.86 [1.22, 2.32]	-0.35 [-1.98, 0.71]
fixedLR	$\alpha_{fixed}$	0.96 [0.86, 0.97]	0.63 [0.37, 0.73]	0.33 [0.19, 0.49]***
RB + fixedLR	H	0.27 [0.00, 0.84]	0.02 [0.00, 0.13]	0.14 [0.00, 0.64] <sup>†</sup>
	K	7.76 [2.18, 9.99]	3.83 [2.36, 9.02]	0.26 [-0.68, 5.77]
	$\alpha_{fixed}$	0.97 [0.75, 1.00]	0.93 [0.23, 1.00]	0.02 [-0.10, 0.56]
	w	0.41 [0.15, 0.79]	0.65 [0.40, 0.87]	-0.23 [-0.57, 0.24]
RB + P <sub>stay</sub>	H	0.86 [0.73, 0.94]	0.35 [0.11, 0.60]	0.47 [0.18, 0.72]**
	K	4.54 [0.12, 9.99]	2.09 [1.51, 4.71]	0.02 [-1.33, 6.41]
	P <sub>stay</sub>	0.00 [0.00, 0.05]	0.01 [0.00, 0.13]	0.00 [-0.11, 0.02]

911 Parameter values were shown as median [IQR]. Difference of parameter values between the two  
 912 conditions was tested by a sign test. <sup>†</sup> $p < 0.08$ , \*\* $p < 0.01$ , \*\*\* $p < 0.001$ .

913

914 Table 3

915 Summary of fMRI results: error magnitude and past error

Cluster index	#Voxels	Region	Peak <i>t</i>	Peak <i>x</i>	Peak <i>y</i>	Peak <i>z</i>
Error magnitude: high-noise versus unstable						
1	21032	R Precuneus	5.22	16	-56	12
		R Angular gyrus	5.17	44	-70	32
		L Precuneus	5.08	-18	-58	20
		Occipital pole	5.07	2	-98	-2
		L Superior parietal lobule	4.91	-10	-66	48
		R Occipital cortex	4.69	26	-76	18
		L Occipital cortex	4.54	-38	-86	26
		R Superior parietal lobule	4.44	44	-44	54
		Posterior cingulate cortex	4.43	2	-46	20
Past error on ambiguous feedback: high-noise versus unstable						
1	1881	Posterior cingulate cortex	4.79	12	-24	52
		R Superior parietal lobule	4.04	32	-38	54
		R Precuneus	3.58	6	-54	70
		L Superior parietal lobule	3.54	-16	-54	62
Conjunction: Error magnitude & Past error on ambiguous feedback						
1	304	R Superior parietal lobule	3.41	38	-40	52
2	103	R Precuneus	3.02	2	-58	70
3	81	L Superior parietal lobule	3.23	-18	-56	72

916



917 Table 4

918 Summary of fMRI results: behavior change

Cluster index	#Voxels	Region	Peak <i>t</i>	Peak <i>x</i>	Peak <i>y</i>	Peak <i>z</i>
Switch versus stay on ambiguous feedback in the high-noise condition						
1	12042	Middle cingulate cortex	4.35	14	-8	30
		R Insula	4.33	38	4	2
		Medial orbitofrontal cortex	4.24	-4	50	-10
		R Frontal pole	4.11	40	46	0
		R Inferior frontal gyrus	4.11	48	26	10
		L Frontal pole	4.01	-24	52	-2
		Dorsomedial frontal cortex	3.96	0	26	34
		Posterior cingulate cortex	3.93	2	-28	50
		R Precentral gyrus	3.91	48	-6	50
		Anterior cingulate cortex	3.51	0	48	20
2	3134	L Precentral gyrus	4.43	-62	2	24
		L Superior temporal gyrus	4.28	-50	-32	12
		L Postcentral gyrus	3.61	-50	-26	44

919